Effect of Silica Nanoparticles on the Fatigue Life of a Glass Fiber Reinforced Epoxy Composite Under an Aircraft Spectrum Load Sequence

N. Jagannathan, K. Sakthivel, Ramesh Bojja and C. M. Manjunatha

Abstract Two types of glass fiber reinforced plastic (GFRP) composites viz., (i) GFRP employing unmodified LY556 epoxy matrix (GFRP-neat), and (ii) GFRP incorporated with 10 wt% of well-dispersed silica nanoparticles in the LY556 epoxy matrix (GFRP-nano), were tested to determine their fatigue life under mini-FALSTAFF, a standard fighter aircraft spectrum load sequence. Spectrum fatigue tests were conducted on standard test specimens in a 50 kN servo-hydraulic test machine with sinusoidal waveform at an average frequency of 3 Hz. Tests were conducted on both types of GFRP composites with various reference stresses to determine the fatigue life expressed as number of blocks required for failure. The fatigue life of GFRP-nano composite was observed to be about four times higher than that of GFRP-neat composite over the entire range of reference stresses investigated. For a given number of applied load cycles, both the matrix crack density and stiffness reduction rates were observed to be lower in GFRP-nano composite when compared to that of GFRP-neat composite. Presence of silica nanoparticles in the epoxy matrix of GFRP appear to reduce matrix cracking and also retard crack growth rate in the composite leading to enhanced fatigue life. Further, using constant fatigue life diagrams of these materials, the spectrum fatigue life under mini-FALSTAFF load sequence was predicted. Good correlation was observed between the predicted and experimental fatigue life for both types of composites.

Keywords Glass fiber · Polymer composite · Spectrum fatigue
Silica nanoparticle

N. Jagannathan (✉) · K. Sakthivel · R. Bojja · C. M. Manjunatha
Structural Technologies Division, Fatigue and Structural Integrity Group,
CSIR-National Aerospace Laboratories, Bengaluru 560017, India
e-mail: njagan@nal.res.in

R. Prakash et al. (eds.), *Advances in Structural Integrity*,
https://doi.org/10.1007/978-981-10-7197-3_3

1 Introduction

Continuous fiber reinforced polymer (FRP) composites are replacing conventional metallic alloys in many structural applications such as airframe, wind turbine, ship hull. Since engineering structures experience cyclic fatigue loads in service, the fatigue performance of such composites assumes significant importance in design, safety, damage tolerance, and durability issues of these structures. Although FRP composites exhibit high specific strength and stiffness with good fatigue resistance, the continuous demand for high-performance structural materials has resulted in use of nanotechnology to further improve mechanical properties of composites.

FRP composites containing nano fillers in the epoxy matrix, called as nanocomposites, have gained tremendous importance in recent times [1, 2]. Significant improvements in static mechanical properties such as tensile and compressive strength, stiffness, interlaminar shear strength, flexural strength, and fracture toughness have been obtained by addition of various types of nanofillers such as SiO_2, SiC, Al_2O_3, and TiO_2 particles, carbon nanotubes, and carbon nanofiber [3–10]. Epoxies modified with layered fillers such as clay, graphite platelets, and fullerene have also been shown to improve the mechanical properties of epoxies and FRPs based upon such modified epoxies [11–15].

The fatigue behavior of bulk epoxies modified with nanofillers has been investigated. Presence of silica nanoparticles, carbon nanotubes, and carbon nanofibers in the epoxy improves constant amplitude fatigue life [16–19]. Further, the use of nano-modified epoxies as the matrices in FRPs has been observed to improve the fatigue properties of the FRPs. The addition of small amounts of carbon nanotubes [20], carbon nanofiber [21], silica nanoparticles [16, 22], and nanoclay [12] has been shown to enhance the fatigue properties of FRP composites.

Hybrid-modified epoxy composites wherein two or more different types or sized fillers added have been developed recently which dramatically improve fracture toughness and fatigue properties of polymer composites. Various hybrid combinations such as nano- and micro-sized silica particles [23], nano-silica and nano-rubber [17], nano-silica and micron rubber [24–28], nano-silica and MWCNT [29], carbon nanotubes and graphite nanoplatelets [30] have been employed to significantly improve fracture toughness and fatigue properties of composites.

Most of the fatigue studies on nanocomposites have been limited to constant amplitude fatigue but spectrum fatigue studies which simulate real service loads have not been studied in detail. Recently, we have observed that a polymer nanocomposite containing silica nanoparticles exhibit improved constant amplitude fatigue life [16] as well as enhanced fatigue life under a wind turbine spectrum load sequence [31]. The main aim of this investigation was to measure and predict the fatigue behavior of a GFRP-nano composite, under a standard aircraft spectrum load sequence. Fatigue life was determined experimentally and compared with predictions through empirical equations.

2 Experimental

2.1 Material

Two types of glass fiber reinforced polymer (GFRP) composites were considered in this study viz., (i) GFRP with unmodified LY556 epoxy matrix (termed as GFRP-neat), and (ii) GFRP with modified epoxy matrix containing 10 wt% silica nanoparticles (termed as GFRP-nano). The complete details of the materials used and the processing employed to fabricate the GFRP composites can be found in Manjunatha et al. [16]. However, for the sake of completeness, they are briefly explained here.

The epoxy resin used was a diglycidyl ether of bisphenol A (DGEBA) resin. The silica (SiO_2) nanoparticles were obtained as a colloidal silica sol. with a concentration of 40 wt% in a DGEBA resin. The curing agent was an accelerated methylhexahydrophthalic acid anhydride. The E-glass fiber cloth used was a non-crimp-fabric. The required quantity of the neat epoxy resin and the calculated quantities of silica nanoparticle-epoxy resin to give 10 wt% of nano-silica in the final resin were all individually weighed, degassed, and mixed together, and a stoichiometric amount of curing agent was added to produce a resin mix. This resin mixture was used to prepare the GFRP composite laminate by resin transfer molding technique.

E-glass fiber fabric pieces were cut and laid up in a quasi-isotropic sequence $[(+45/-45/0/90)_s]_2$. The resin mixture was infused into the glass-cloth layup and cured at 100 °C for 2 h and post-cured at 150 °C for 10 h. In this way, two types of GFRP composites were fabricated, i.e., GFRP-neat and GFRP-nano. The laminates produced were about 2.5–2.7 mm thick and had a fiber volume fraction of about 57%.

The silica particles of about 20 nm in diameter were evenly distributed in the epoxy as shown in atomic force microscopic image [16] in Fig. 1. The tensile and compressive properties of the composite laminates [31] are shown in Table 1. Both the strength and stiffness of GFRP-nano composite are slightly higher in both tension and compression due to the presence of hard silica nanoparticles in the epoxy matrix.

2.2 Fatigue Testing

Fatigue tests on composites were conducted under a standard spectrum load sequence. The load sequence considered in this investigation was a fighter aircraft loading standard for fatigue evaluation, mini-FALSTAFF [32, 33] shown in Fig. 2. It is a short version of standard FALSTAFF load spectrum, which is a standardized variable-amplitude test load sequence developed for the fatigue analysis of materials used for fighter aircraft. In Fig. 2, the normalized stress is plotted against peak/

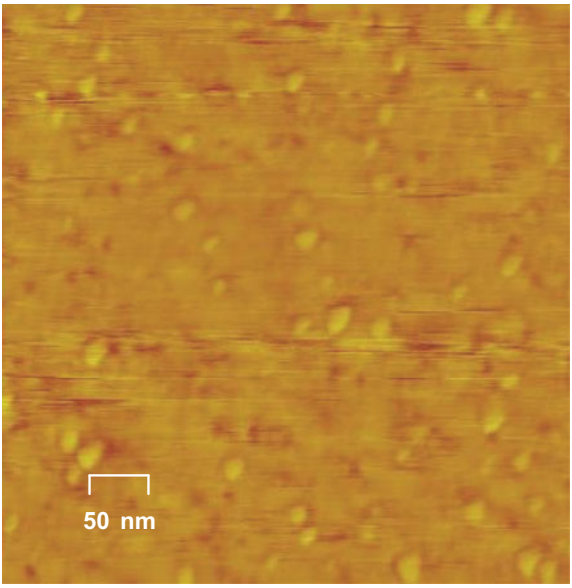

Fig. 1 Atomic force microscopy image of a 10 wt% silica nanoparticle-modified bulk epoxy polymer [31]

Table 1 Mechanical properties of the GFRP composites [31]

Type of test	Mechanical property	Material		% change
		GFRP-neat	GFRP-nano	
Tension	σ_{UTS} (MPa)	365 ± 13	382 ± 12	+4.65
	E_T (GPa)	17.5 ± 0.1	18.8 ± 1.7	+7.42
Compression	σ_{UCS} (MPa)	355 ± 47	361 ± 28	+1.69
	E_C (GPa)	21.3 ± 0.4	22.6 ± 0.4	+6.10

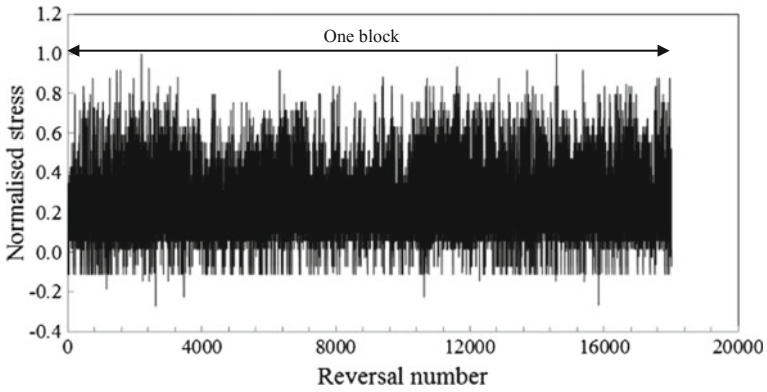

Fig. 2 Standard mini-FALSTAFF spectrum load sequence [32]

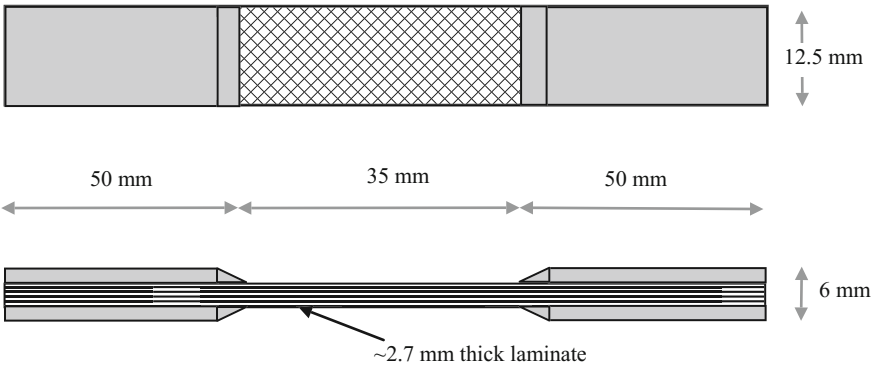

Fig. 3 Schematic diagram showing the dimensions of the fatigue test specimens

trough points of load sequence. One block of this load sequence consists of 18,012 reversals at 32 different stress levels and represents loading equivalent of 200 flights. The stress sequence for our experiments was obtained by multiplying with a constant reference stress value, σ_{ref} for all the peak/trough points in the entire block.

Spectrum fatigue tests with various reference stress levels were conducted on both GFRP composites. The geometry and dimensions of the test specimens employed for spectrum fatigue tests are shown in Fig. 3. Tests were conducted in a computer controlled 50 kN servo-hydraulic test machine. Sinusoidal waveform with an average frequency of 3 Hz (six reversals per second) was employed in the tests. For any given reference stress, the number of load blocks required to fail the test specimen, N_b, was determined. Whenever a specimen failed in-between a full block, it was rounded-off to the nearest complete block number.

The stiffness variation of the specimen subjected to spectrum fatigue loads was determined during the test as a function of the number of applied load blocks. Whenever stiffness measurement data were required, the fatigue test was intermittently stopped, a load cycle with $\sigma_{max} = 0.5\ \sigma_{ref}$ and stress ratio $R = \sigma_{min}/\sigma_{max} = 0$ was applied, the load versus displacement data were obtained and then analyzed. Considering the large number of load cycles in one block, insertion of this one cycle was assumed not to alter the fatigue damage in the material significantly. For the purpose of comparison, the normalized stiffness of the specimen was defined as the ratio of measured stiffness at any given time to the initial stiffness (obtained before application of the first spectrum load block). For one particular test with $\sigma_{ref} = 250$ MPa, the specimens were dismounted at the end of the application of three complete load block, and photographs showing matrix cracks were obtained, as explained in [16].

2.3 Fatigue Life Prediction

The fatigue life of the GFRP composites under the mini-FALSTAFF load sequence was predicted and compared with the experimental results. The general methodology followed in prediction of fatigue life under spectrum loads in composites may be found elsewhere [31, 34]. A schematic of flow chart for life prediction is shown in Fig. 4 which involves [31]: (i) the rainflow counting of the fatigue cycles in the spectrum load sequence, (ii) the determination of the cycles to failure, N_f, for each of the counted load cycles using a constant life diagram (CLD) of the material, (iii) the calculation of the damage fraction for each of the counted load cycles as the ratio of cycle count to N_f obtained from the CLD, and finally (iv) the determination of the total fatigue damage per load block by summation of the damage fraction. The material is assumed to fail when the total damage fraction reaches 1.0, and, hence, the fatigue life under the spectrum load sequence is equal to the reciprocal of the total damage estimated per load block. This procedure was followed in the present study for estimation of fatigue life.

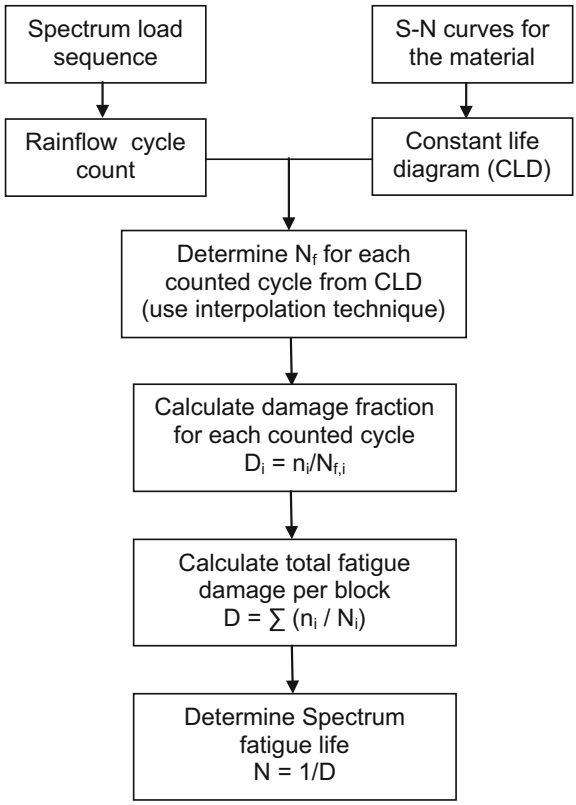

Fig. 4 Schematic diagram showing the procedure for prediction of spectrum fatigue life [31]

3 Results and Discussion

3.1 Experimental Spectrum Fatigue Life

The experimentally determined spectrum fatigue life of GFRP composites under mini-FALSTAFF load sequence at various reference stresses is shown in Fig. 5. The fatigue life was observed to increase with a reduction in the reference stress in both GFRP composites, as observed in many other investigations [31, 35, 36]. It may also be seen that for any given reference stress level, the GFRP-nano composite shows higher fatigue life compared to that of GFRP-neat composite by about three times. The spectrum fatigue life enhancement is observed over the entire range of reference stress levels investigated.

The normalized stiffness of the specimen as a function of spectrum load blocks determined for the fatigue test with σ_{ref} = 250 MPa, for both GFRP composites is shown in Fig. 6. The stiffness reduction trend observed in these materials is similar to generally observed behavior in FRP composites [37–42]. It may be seen that the stiffness reduction rate is quite high in the GFRP-neat composite than in GFRP-nano composite.

Photographs of the matrix cracks observed on the surface of the composite subjected to thee complete load block of the mini-FALSTAFF spectrum load sequence with σ_{ref} = 250 MPa are shown in Fig. 7. Initiation and growth of such matrix cracks under cyclic fatigue loads in GFRP composite have been reported by others [16, 42]. The GFRP-neat composite exhibits more severe cracking than GFRP-nano composite suggesting suppression of matrix cracks by nano modification of epoxy matrix.

The fatigue failure mechanisms under cyclic loads in polymer composites have been investigated extensively. The generally accepted mechanisms include [37, 40] (i) initiation and growth of matrix cracks, (ii) initiation and growth of disbonds and delaminations, and (iii) individual fiber breaks throughout the fatigue life. Studies have clearly shown that the fatigue crack growth rate of the bulk epoxy containing

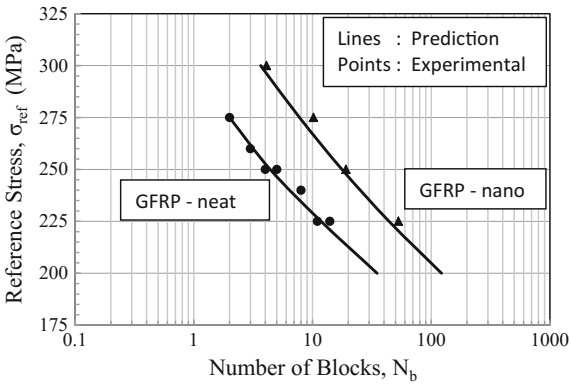

Fig. 5 Experimental and predicted fatigue lives of the GFRP composites under the mini-FALSTAFF spectrum load sequence

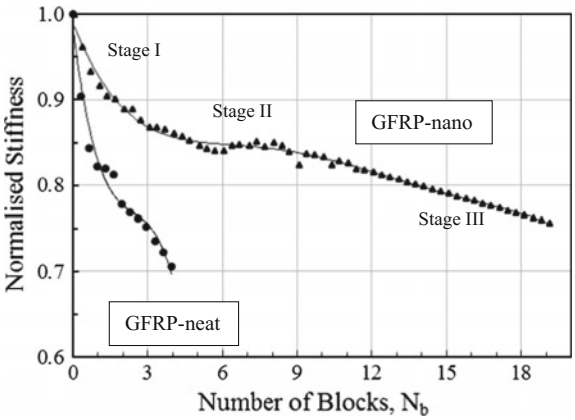

Fig. 6 Variation of the normalized stiffness for the GFRP composites determined under the mini-FALSTAFF spectrum load sequence, with σ_{ref} = 250 MPa

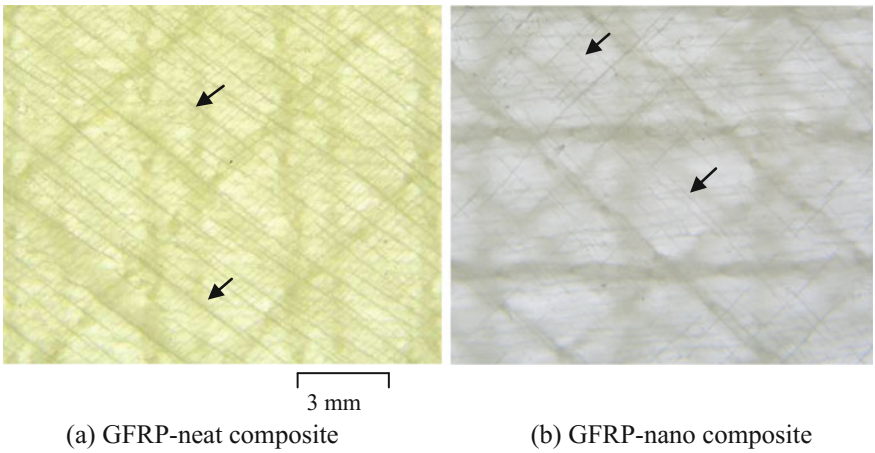

Fig. 7 Photographs showing matrix cracks (indicated by the arrows) in the GFRP composites subjected to three complete mini-FALSTAFF spectrum load blocks with σ_{ref} = 250 MPa

nano-silica particles is over an order of magnitude lower than that of the neat epoxy [43, 44]. Further, it has been shown that the use of such particles to formulate a modified epoxy matrix in a GFRP composite material enhances the constant amplitude fatigue life due to suppressed matrix cracking, delayed initiation of delamination, and reduced crack/delamination growth rate [16].

The stiffness loss in stage I and stage II results primarily from matrix cracking. Once the matrix crack density saturates and attains the characteristic damage state (CDS), the disbonds and delaminations created due to the coalescence of primary and secondary matrix cracks grow, and this leads to a further loss in stiffness. The

present results show that when both composites are subjected to the same number of spectrum load blocks, the crack density is lower in the GFRP-nano composite compared to the GFRP-neat composite. Thus, the stiffness loss curves shown in Fig. 6 indicate the underlying mechanisms, i.e., suppressed matrix cracking, delayed initiation of delamination, and a reduced crack/delamination growth rate. All these mechanisms lead to an improvement in the spectrum fatigue life of the GFRP-nano composite.

3.2 Spectrum Fatigue Life Prediction

The fatigue life of GFRP-neat and GFRP-nano composites was predicted following the procedure shown in Fig. 4. The constant life diagrams (CLDs) for the GFRP composites determined in an earlier investigation [31] are shown in Fig. 8. Rainflow counting of the fatigue cycles in the spectrum load sequence was performed following the ASTM standard specified procedure [45]. Since each of the rainflow-counted load cycles will be of different load amplitude and mean stress, it is necessary to interpolate and determine N_f for all these load cycles using the CLD. A piecewise linear interpolation technique [46] was used in the present investigation. For damage accumulation model, the Miners' linear damage accumulation rule [47] was used:

$$D = \sum (n_i/N_i) \tag{1}$$

where D is the damage fraction, n_i is the cycle count, and N_i is the cycles to failure for a given load cycle amplitude. Thus, the total damage per load block was estimated following the above procedure, and the spectrum fatigue life was predicted for the GFRP composites.

The fatigue life predicted as a function of the reference stress following the above procedure is shown in Fig. 5, along with the experimental results. It may be observed from these results that very good agreement exists between the experimental and the predicted fatigue lives for both GFRP composites. Thus, the predictions also suggest an improvement in the fatigue life of GFRP-nano composite by about four times over that of GFRP-neat composite.

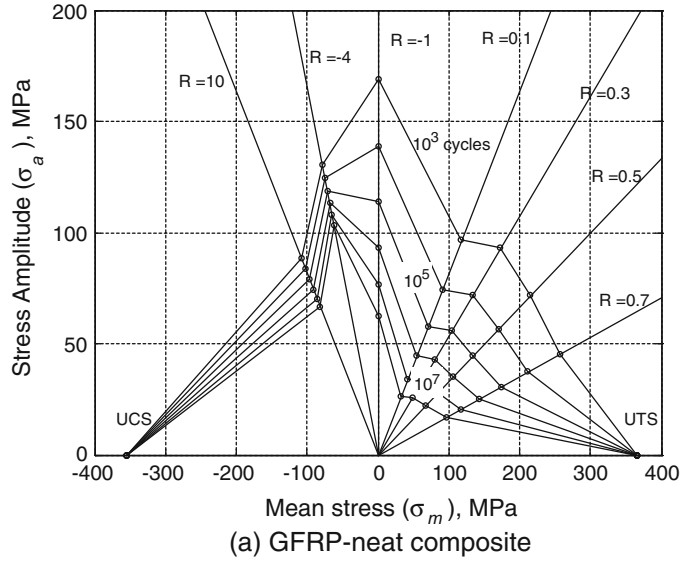

(a) GFRP-neat composite

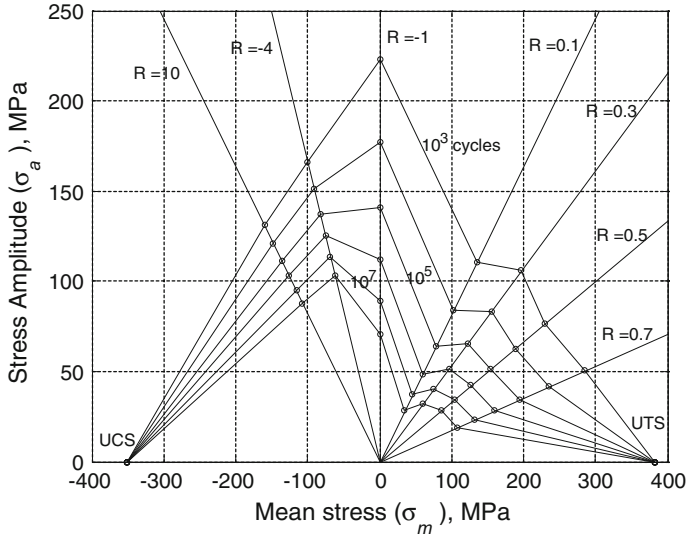

(b) GFRP-nano composite

Fig. 8 Constant life diagrams (CLDs) for the GFRP composites [31]

4 Conclusions

Based on the results obtained in this investigation, the following conclusions may be drawn:

1. The addition 10 wt% of silica nanoparticles to the epoxy matrix of a GFRP composite improves the fatigue life under mini-FALSTAFF spectrum load sequence by about four times.
2. The suppressed matrix cracking and retarded crack and delamination growth rate in the silica nanoparticle-modified epoxy matrix of the GFRP composite appear to enhance the spectrum fatigue life.
3. The predicted fatigue lives under the mini-FALSTAFF spectrum load sequence are in very good agreement with the experimental observations for both the GFRP-neat and GFRP-nano composites.

Acknowledgements The authors from CSIR-NAL wish to thank Mr. Shyam Chetty, Director and Dr. Satish Chandra, Head, Structural Technologies Division, CSIR-National Aerospace Laboratories, Bangalore, India, for their constant support and encouragement during this work. The laminates were fabricated in the department of Mechanical Engineering, Imperial College, London, UK. Thanks to Prof. A.J. Kinloch and Dr. A.C. Taylor for their assistance and encouragement during this work. The authors also wish to thank the technical support staff members of the Department of Mechanical Engineering and the Composites Centre of the Aeronautics Department, Imperial College London, and the Materials Evaluation Lab, STTD, NAL, Bangalore, for their assistance in the experimental work.

References

1. E.T. Thostenson, C. Li, T.W. Chou, Comp. Sci. Tech. **65**, 491 (2005)
2. F. Hussain, M. Hojjati, M. Okamoto, R.E. Gorga, J. Comp. Mater. **40**, 1511 (2006)
3. J. Ma, M.S. Mo, X.S. Du, P. Rosso, K. Friedrich, H.C. Kuan, Polymer **49**, 3510 (2008)
4. C.M. Manjunatha, A.C. Taylor, A.J. Kinloch, S. Sprenger, J. Mater. Sci. **44**(16), 4487 (2009)
5. N. Chisholm, H. Mahfuz, V.K. Rangari, A. Ashfaq, S. Jeelani, Compos. Struct. **67**, 115 (2005)
6. S. Zhao, L.S. Schadler, H. Hillborg, T. Auletta, Compos. Sci. Tech. **68**, 2976 (2008)
7. B. Wetzel, P. Rosso, F. Haupert, K. Friedrich, Eng. Fract. Mech. **73**, 2375 (2006)
8. F.H. Gojny, M.H.G. Wichmann, B. Fiedler, W. Bauhofer, K. Schulte, Compos. A: Appl. Sci. Manufac. **36**, 1525 (2005)
9. Z. Spitalsky, D. Tasis, K. Papagelis, C. Galiotis, Prog. Polym. Sci. **35**, 357 (2010)
10. C.M. Manjunatha, A.C. Taylor, A.J. Kinloch, S. Sprenger, J. Mater. Sci. **44**(1), 342 (2009)
11. Y. Zhou, V. Rangari, H. Mahfuz, S. Jeelani, P.K. Mallick, Mater. Sci. Eng. A **402**, 109 (2005)
12. S.U. Khan, A. Munir, R. Hussain, J.K. Kim, Compos. Sci. Tech. **70**, 2077 (2010)
13. Y. Zhou, M. Hosur, S. Jeelani, P. Mallick, J. Mater. Sci. **47**, 5002 (2012)
14. J. Cho, J.Y. Chen, I.M. Daniel, Script. Mater. **56**, 685 (2007)
15. A.M. Rafiee, F. Yavari, J. Rafiee, N. Koratkar, J. Nano. Part Res. **13**, 733 (2011)
16. C.M. Manjunatha, A.C. Taylor, A.J. Kinloch, S. Sprenger, Compos. Sci. Tech. **70**, 193 (2010)
17. G.T. Wang, H.Y. Liu, N. Saintier, Y.W. Mai, Eng. Fail. Analy. **16**, 2635 (2009)
18. N. Yu, Z.H. Zhang, S.Y. He, Mater. Sci. Eng. A **494**, 380 (2008)

19. D.R. Bortz, C. Merino, I. Martin-Gullon, Compos. Sci. Tech. **71**, 31 (2011)
20. C. Grimmer, C. Dharan, J. Mater. Sci. **43**, 4487 (2008)
21. D.R. Bortz, C. Merino, I. Martin-Gullon, Compos. Sci. Tech. **72**, 446 (2012)
22. L. Böger, J. Sumfleth, H. Hedemann, K. Schulte, Compos. Part A: Appl. Sci. Manufact. **41**, 1419 (2010)
23. T. Adachi, M. Osaki, W. Araki, S.C. Kwon, Acta Mater. **56**, 2101 (2008)
24. Y.L. Liang, R.A. Pearson, Polymer **51**, 4880 (2010)
25. A.J. Kinloch, R.D. Mohammed, A.C. Taylor, C. Eger, S. Sprenger, D. Egan, J. Mater. Sci. **40**, 5083 (2005)
26. A.J. Kinloch, R.D. Mohammed, A.C. Taylor, S. Sprenger, D.J. Egan, J. Mater. Sci. **41**, 5043 (2006)
27. A.J. Kinloch, K. Masania, A.C. Taylor, S. Sprenger, D. Egan, J. Mater. Sci. **43**, 1151 (2008)
28. C.M. Manjunatha, S. Sprenger, A.C. Taylor, A.J. Kinloch, J. Compos. Mater. **44**, 2095 (2010)
29. L. Böger, J. Sumfleth, H. Hedemann K. Schulte, Compos. Part A: Appl. Sci. Manufact. **41**, 1419 (2010)
30. J. Li, P.S. Wong, J.K. Kim, Mater. Sci. Eng. A **483**, 660 (2008)
31. C.M. Manjunatha, R. Bojja, N. Jagannathan , Mater. Perf. Char. **3**(1), 327 (2014)
32. G.M. Van Dijk, J.B. de Jonge, National Aerospace Laboratory NLR, Netherlands, NLR MP 75017 U (1975)
33. P. Heuler, H. Klatschke, Int. J. Fat. **27**, 974 (2005)
34. N.L. Post, S.W. Case, J.J. Lesko, Int. J. Fat. **30**, 2064 (2008)
35. T.P. Philippidis, A.P. Vassilopoulos, Compos. Part A: Appl. Sci. Manufact. **35**, 657 (2004)
36. C.M. Manjunatha, Ramesh Bojja, N. Jagannathan, A.J. Kinloch, A.C. Taylor, Int. J. Fat. **54**, 25 (2013)
37. R. Talreja, Proc. Roy. Soc. London. A. Math. Phys. Sci. **378**, 461 (1981)
38. J.S. Tate, A.D. Kelkar, Compos. B **39**, 548 (2008)
39. K.L. Reifsnider, R. Jamison, Int. J Fat. **4**, 187 (1982)
40. S.W. Case, K.L. Reifsnider, in *Fatigue of Composite Materials*, eds. I. Milne, R.O. Ritchie, B. Karihaloo. Comprehensive Structural Integrity, vol. 4 Cyclic loading and fatigue, (Elsevier Science, Amsterdam, 2003)
41. A. Gagel, B. Fiedler, K. Schulte, Compos. Sci. Tech **66**, 657 (2006)
42. A. Gagel, D. Lange, K. Schulte, Compos. A **37**, 222 (2006)
43. H.Y. Liu, G. Wang, Y.W. Mai, Compos. Sci. Tech. **72**(13), 1530 (2012)
44. C.M. Manjunatha, N. Jagannathan, K. Padmalatha, A.C. Taylor, A.J. Kinloch, Int. J. Nanosci. **10**, 1095 (2011)
45. Standard Practices for Cycle Counting in Fatigue Analysis, ASTM E1049, Annual book of ASTM Standards, American Society for Testing and Materials, PA, vol. 15.03, (2003)
46. A.P. Vassilopoulos, B.D. Manshadi, T. Keller, Int. J. Fat. **32**, 659 (2010)
47. M.A. Miner, J. Appl. Mech. **12A**, 159 (1945)